Department of Veterans Affairs

Journal of Rehabilitation Research and Development Vol. 37 No. 4, July/August 2000
Pages 405–413

Experimental and numerical predictions of the ultimate strength of a low-cost composite transtibial prosthesis

Jill Hahl, MS and Minoru Taya, PhD
Center for Intelligent Materials and Systems, Department of Mechanical Engineering, University of Washington, Seattle, WA 98195-2600

Abstract—Saito et al. (Modern Plastics 1997;74:175–7) have developed a low-cost transtibial prosthesis made of fiber-reinforced plastic (FRP). The prosthesis is comprised of an aluminum pylon, a cosmetic cover, and a constant cross-section composite foot into which aluminum supports are screwed to increase load-bearing capacity. Replacing these supports with a single integrated FRP stiffener significantly reduced manufacturing cost while providing high strength, great durability, and smooth walking. The optimal location and orientation of the proposed FRP stiffener were determined by finite element (FE) analysis. When a replica of this component was tested according to ISO standard 10328, the experimental prosthesis catastrophically failed under 6600 N of force. Maximum percent error of strain between experimental and numerical results was 18.6%, showing good correlation between the two data sets. The optimized design provides sufficient strength and reduces the cost of manufacturing and thus can be used to replace the original design.

Key words: *composite, finite element analysis, prosthesis, transtibial.*

This material is based upon work supported by Kobe Steel Ltd., 5-5, Takatsukadia, 1-chrome, Nishi-ku Kobe, HYOGO, 651-22 Japan.

Address all correspondence and requests for reprints to Jill Hahl, MS, Center for Intelligent Materials and Systems, Department of Mechanical Engineering, University of Washington, Seattle, WA 98195-2600; email: jhahl@u.washington.edu.

INTRODUCTION

Several million people living in Third World countries are in need of lower leg prostheses but are unable to afford the high costs of current prosthetic components. Various humanitarian aid programs throughout the world can provide artificial legs to those in need. However, due to the high cost of the current Western components the number of donations is limited. Thus people living in these areas are forced to resort to crude imitations constructed from wood or bamboo without regard to comfort or safety standards (1). As the high costs associated with prosthetic limbs are due primarily to small-scale production methods, mass producing the components is a key to lowering manufacturing costs. Saito et al. (1) have developed a mass-produced, transtibial fiber-reinforced plastic (FRP) prosthesis with a design that incorporates low manufacturing costs, high strength, great durability, and smooth walking.

The basic design for the prosthetic leg consists of an axial structural member, a foot component, and a cosmetic cover (**Figure 1**). A simple 6061-T6-aluminum pipe is used for the axial member. The foot component consists of an FRP composite shell of constant cross section. The composite is made of a vinyl ester resin reinforced with E-glass fibers. The shell is formed by pultrusion, a con-

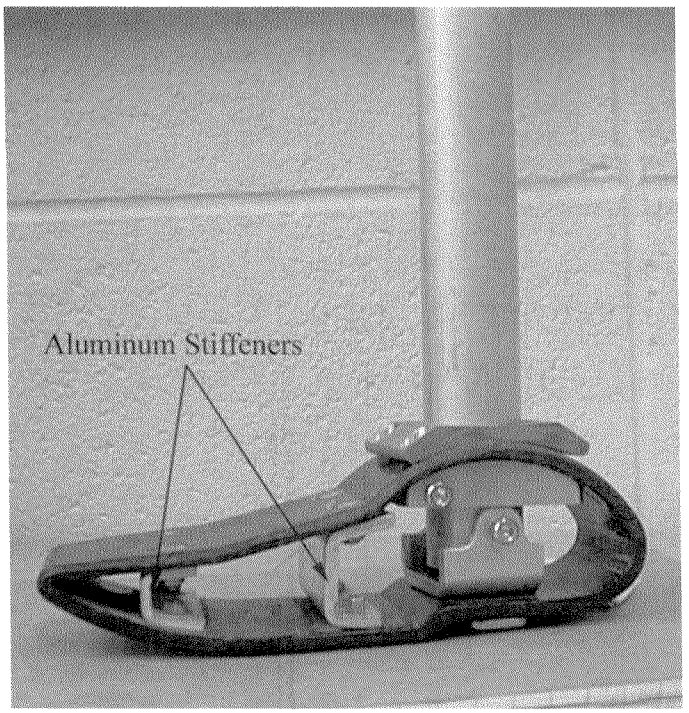

Figure 1.
Original prosthesis as designed by Saito et al. (1).

ventional industrial forming process ideal for producing low-cost composite structures of uniform cross section. A plastic cosmetic cover, resembling the biological foot, is placed over the prosthesis.

A schematic of the pultrusion process used to build the foot section of the prosthesis is shown in **Figure 2**. Continuous mats are pulled from one end of the line through a resin bath, the viscosity of which is precisely controlled to ensure proper wetting of the fibers. After the resin bath, the semi-liquid product is coated with a surface veil for protection. It is then pulled through the preformer, which is responsible for squeezing out excess resin, distributing the fibers evenly, and bringing the material into its final configuration. The product then enters the die where final curing, shaping, and compaction take place. Cutting the pultruded material into individual slices creates the final product (2).

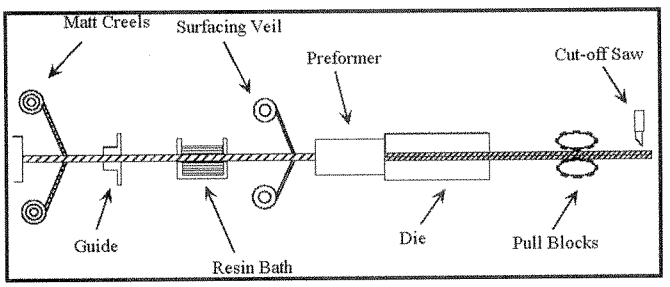

Figure 2.
Schematic of the pultrusion process.

Figure 3 shows the basic design of the rigid foot component. If the prosthesis is to reproduce the motions of the intact limb adequately, the prosthetic ankle must follow approximately the same path as that traced by the biological joint during gait. The radius, R, and length, L (as shown in **Figure 3**), were optimized by Saito et al. to simulate the normal gait pattern of the biological foot/ankle complex (1). For optimal fit and use, the patient can adjust the inclination of the axial pipe. A small piece of FRP is attached to the heel section of the foot component for shock absorption during heel strike.

Vertical aluminum supports in the midfoot and forefoot region were incorporated into the foot in order to increase its load-bearing capacity (**Figure 1**). Replacing these aluminum supports with a single pultruded stiffener integrated into the foot shell during pultrusion, however, will allow for reduced costs of manufacturing.

The purpose of this development, then, was to reduce the cost of the prosthesis by incorporating an FRP substitute for the vertical stiffeners during pultrusion of the foot shell, thereby lowering the overall cost of production. The immediate objective of this study was to

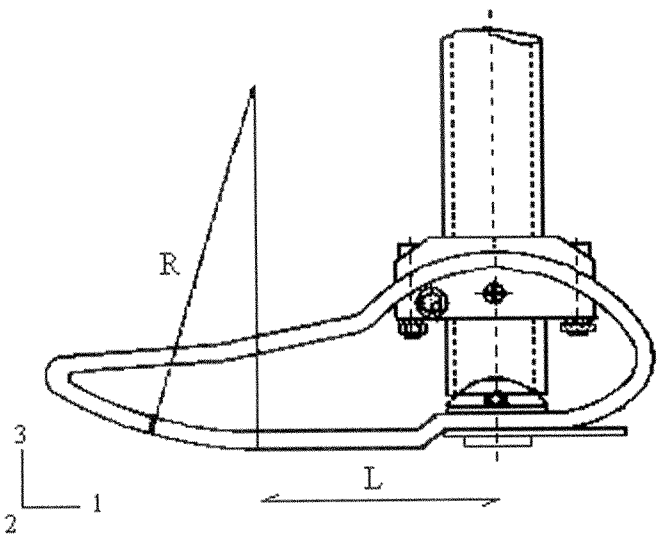

Figure 3.
Basic design of the prosthesis.

determine the optimum location of the FRP stiffener and to test the modified design to ensure that it satisfied the ISO 10328 standard for prostheses (3).

METHODS

Numerical Analysis

The initial stage of the research consisted of using ABAQUS, a finite element (FE) program, to model the prosthesis. The 3-D FE model consisted of over 3000 elements. From the FE analysis, we received output regarding stress and strain distributions within the prosthesis in terms of local coordinates. The element type used was a 3-D shell element. This was a 4-node, doubly curved, general-purpose shell with reduced integration, hourglass control, and finite member strains. The model was used to investigate a series of different loading conditions intended to simulate the stages of loading during the stance phase of gait.

Figure 4 shows the boundary conditions used in the FE model. A rigid surface contact condition was used to simulate the ground surface. The height of the modeled transtibial prosthesis was fixed at 30 cm. The maximum patient weight for the prosthesis was assumed to be 100 kg. A force of 1,000 N, representative of the user's weight, was applied to the top of the prosthesis. Horizontal displacements ranging from 0 to 110 mm (5 mm increments) were used to simulate walking. **Table 1** summarizes the material properties used in the modeling of the prosthesis.

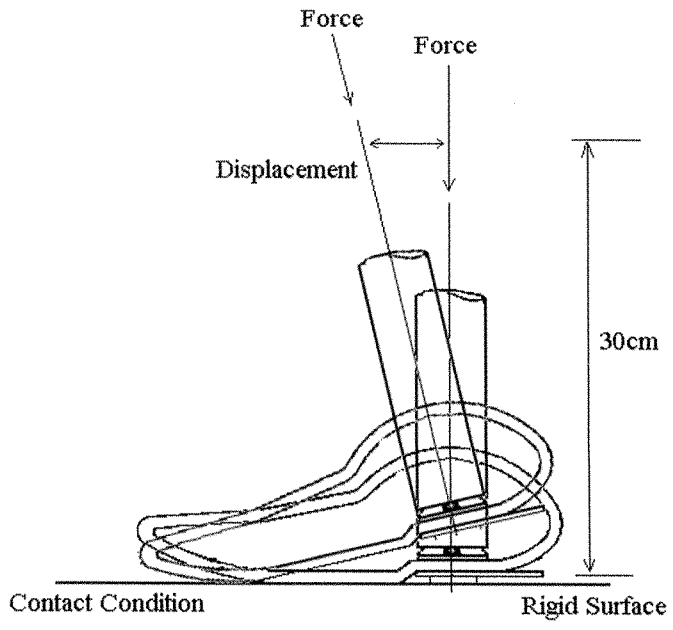

Figure 4.
Boundary conditions for the FE model.

Table 1.
Material properties used in FE model.

Material	Young's Modulus (GPa)	Poisson's Ratio
FRP shell (4)	12.23	0.03
6061-T6 Aluminum pipe (7)	68.9	0.35

The aluminum supports in the ABAQUS model were replaced with FRP stiffeners. Optimization of the location and geometry of the stiffener was determined by numerical analysis using ABAQUS. The optimal placement and rotational angle of the stiffener minimized the maximum strain in the shell. Preferably, the number of stiffeners would be reduced from two to one in order to facilitate the manufacturing procedure. Many different stiffener placements and angles were examined. This process is described in detail in the literature (4). **Figure 5** is a sketch of the optimized prosthesis. Using ABAQUS, the optimum stiffener placement was found to be between the two original aluminum stiffeners (39.5 mm from the toe) with a clockwise base rotation of 12°.

Failure Analysis

Failure analysis was performed on the optimized design to ensure that it would withstand the loading conditions. The Tsai-Hill Criterion, represented by Equation 1, was used to predict failure (5).

$$C_{th}=\frac{\sigma_1^2}{S_L^2}-\frac{\sigma_1\sigma_2}{S_L^2}+\frac{\sigma_2^2}{S_T^2}+\frac{\tau_{12}^2}{S_{LT}^2} \quad [1]$$

Where SL, ST, STL are the ultimate strengths of E-glass/vinyl ester in the longitudinal, transverse, and shear directions, respectively, and σ_1, σ_2, and τ_{12} are the imposed stresses in the longitudinal, transverse, and shear directions. Failure is avoided for $C_{th}\leq 1$ and failure is predicted for $C_{th}\geq 1$. The Tsai-Hill Criterion is based on the Maximum Distortion Criterion, or Von Mises Criterion, and includes the effects of induced anisotropic behavior (5).

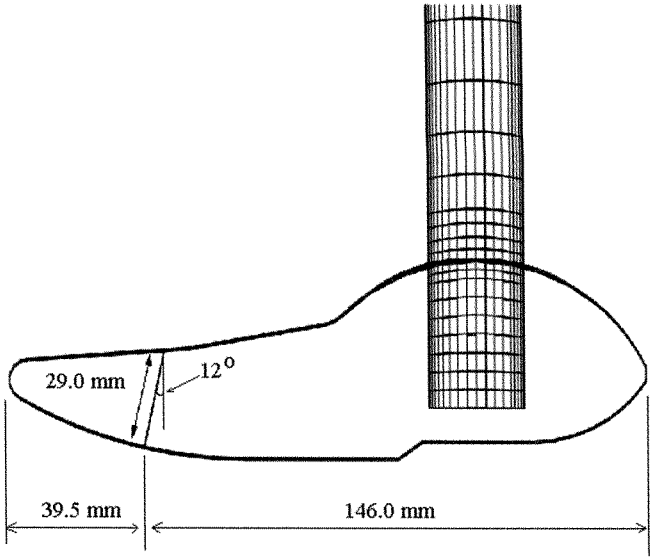

Figure 5.
Optimized design. Shell thickness is 5 mm (including stiffener).

Fabrication

To validate the analytical results, a prototype of the composite foot section of the prosthesis was built using the conventional hand layup (bag molding) procedure for composites. In industry, the foot section of the transtibial prosthesis is mass produced using a process called pultrusion that uses a die to shape the final product. This die is expensive to produce and a new one is required to construct the optimized prosthesis. Thus, it was first necessary to construct a prototype of the prosthesis using the less expensive, bag molding process before investing in a new die for the pultrusion line.

Prepreg, a partially cured E-glass fiber weave/epoxy resin with 38 percent by weight resin content, was used as the starting material for this process. A total of 20 plies of prepreg was wrapped around an aluminum mold and prepared for cure. Teflon intensifiers were placed on the wrapped mold to prevent buildup in the critical areas above and below the stiffener and around the heel section of the foot. A porous release cloth was then wound around the entire assembly followed by bleeder fabric, which is used to absorb the excess resin that flows from the prepreg during curing. A second porous release cloth was then wrapped around the bleeder cloth followed by a thin vacuum bag. A vacuum was created on the foot component and it was placed in the autoclave where a combination of temperature and pressure was applied to consolidate the part into one single laminate.

After curing was complete, the part was removed from the autoclave and allowed to cool for 2 hr. The vacuum bag was then removed and both the bleeder fabric and Teflon coating were carefully stripped from the cured component. Following stripping, the mold was removed from the part. During curing, resin seeped around the sides of the mold. This excess resin was removed from the mold using a very sharp knife. It was necessary to use a press to remove the mold from the cured foot.

The foot section was cut into sections 60 mm in width and these sections were then prepared for assembly with the leg component. To prepare for assembly, several holes were cut in the top section of the composite foot component where the leg was to be inserted. These holes were identical to those used in the Saito et al. design (1).

The aluminum leg was then attached to the composite foot section using a set of aluminum clamps. **Figure 6**

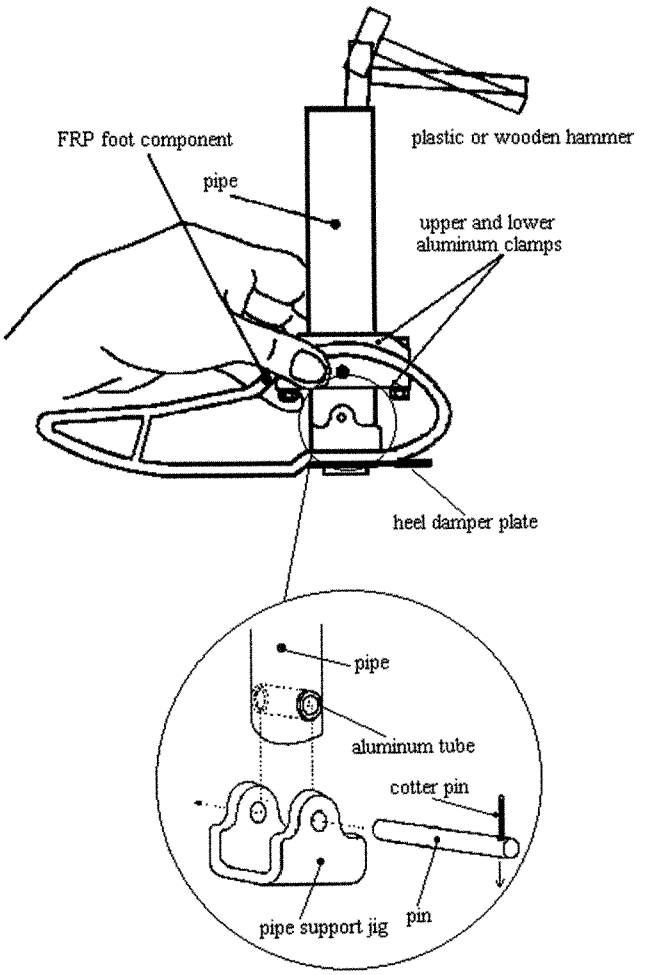

Figure 6.
Assembly of the prosthesis.

depicts the assembly of the prosthesis. The upper and lower aluminum clamps work to connect the aluminum axial member to the foot component of the prosthesis and also prevent rotation of the pipe. It is imperative that this connection be adjusted properly since failure to do so could lead to injury of the user. The inclination of the pipe is adjusted to suit the needs of the patient. This is dependent on his or her height, weight, and gait. Note also that the length of the heel damper plate can be adjusted. The longer the damper plate, the ``softer the feel'' of the heel at contact. These conditions were not of critical importance for mechanical testing of the prosthesis but should be taken into consideration when preparing for patient testing.

Three-element rectangular 45-degree stacked rosette strain gauges (Measurements Group Inc., Raleigh, NC) were used to determine the complete strain field. Using strain contour plots from ABAQUS, appropriate locations for the strain gauges were determined. The optimal locations for the strain gauges were determined by considering the locations of high stress (gauge 1), areas where strain does not vary widely with location (gauge 2), and areas on the stiffener section (gauge 3). **Figure 7** is a sketch of the locations and alignment of the strain gauges. Note that all gauges are along the centerline on the prosthetic component.

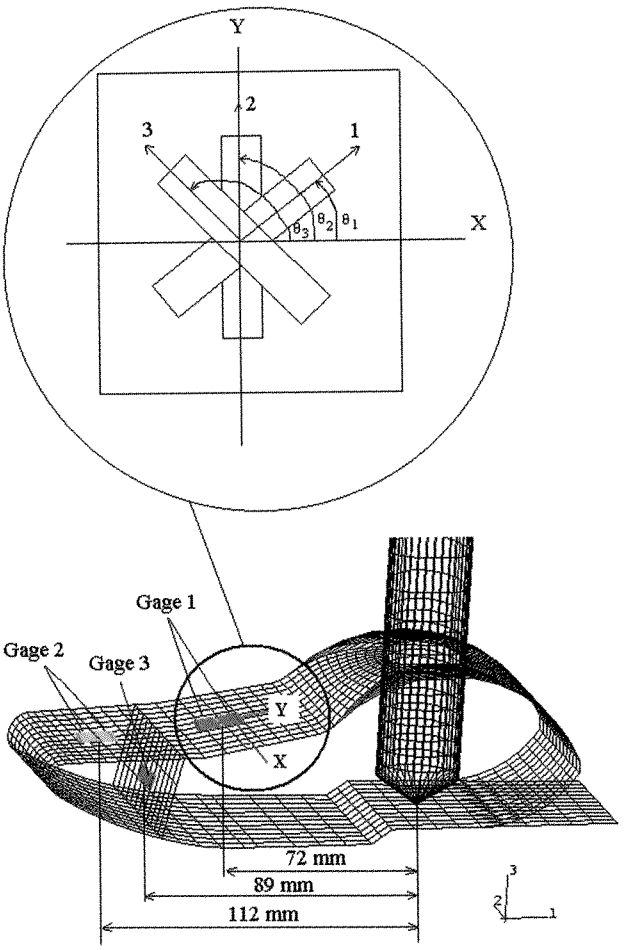

Figure 7.
A sketch of the locations and alignment of the strain gauges. The gauges are positioned along the centerline of the foot component.

Testing

Using the ISO 10328 standard as a guide, two sets of tests were performed on the optimized prosthesis. The test setup consisted of a data acquisition system, a CCD camera, and an Instron mechanical testing machine. **Figure 8** is a photograph of the prosthesis during testing. For both tests, a set of jigs attached to the machine allowed for testing according to the ISO standard 10328 (3). The jigs created compound loading conditions on the prosthesis by the application of a single offset axial force.

First, a failure test was performed on the prosthesis to determine the load at which it will break. The prosthesis was arranged in the jigs at a horizontal displacement of 110 mm, which represents the toe-off condition. A compressive load was applied to the prosthesis using position control at a constant displacement rate of 1 mm/min. The results were then compared to numerical predictions.

A second test was performed where strain was monitored at three separate locations on the FRP foot component while load was applied to the prosthesis. The prosthesis was placed on a flat surface and arranged in the jigs at a horizontal displacement of 10 mm. The jigs were aligned to satisfy the ISO 10328 standard for transtibial prostheses. The prosthesis was subjected to force ranging from 150 N to 450 N. The strains measured using the rosette strain gauges were converted into strains in the Cartesian coordinate system using the following equations (6).

$$\begin{aligned}\varepsilon_{\theta 1}&=\varepsilon_x\cos^2\theta_1+\varepsilon_y\sin^2\theta_1+\gamma_{xy}\cos\theta_1\sin\theta_1\\ \varepsilon_{\theta 2}&=\varepsilon_x\cos^2\theta_2+\varepsilon_y\sin^2\theta_2+\gamma_{xy}\cos\theta_2\sin\theta_2\\ \varepsilon_{\theta 3}&=\varepsilon_x\cos^2\theta_3+\varepsilon_y\sin^2\theta_3+\gamma_{xy}\cos\theta_3\sin\theta_3\end{aligned} \quad [2]$$

where $\epsilon_{\theta 1}$, $\epsilon_{\theta 2}$, and $\epsilon_{\theta 3}$ are the strains measured by the rosettes in the θ_1, θ_2, and θ_3 directions, respectively. ϵ_x, ϵ_y, and γ_{xy} are the normal, transverse, and shear strains, respectively, in the Cartesian coordinate system. The

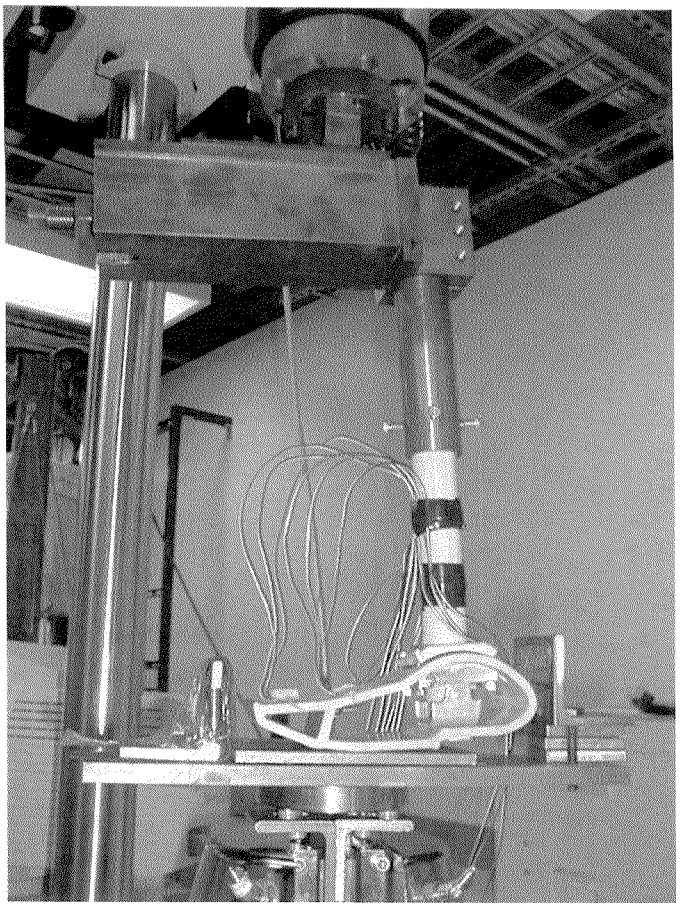

Figure 8.
Photograph of the setup used for mechanical testing of the prosthesis. Satisfies the ISO 10328 Standard.

Cartesian coordinates are directly associated with the local x and y axes as defined by ABAQUS for the FE model.

By employing Equation 3, the principle strains in the composite foot section were determined for each gauge location (7),

$$\varepsilon_{1,2}=\frac{\varepsilon_x+\varepsilon_y}{2}\pm\sqrt{\left(\frac{\varepsilon_x-\varepsilon_y}{2}\right)^2+\left(\frac{\gamma_{xy}}{2}\right)^2} \qquad [3]$$

where ϵ_1 and ϵ_2 are the maximum and minimum principle strains, respectively.

RESULTS

Theoretical Prediction of Failure Load

Failure analysis was performed on the optimized design using the Tsai-Hill Failure Criterion. Equation 1 was applied to areas of highest concern. These areas included the sections of highest stresses and the section where the stiffener contacts the outer shell. Typical values of lamina strengths of the material used in Equation 1 are summarized in **Table 2** (5). Tensile values of the ultimate strengths were used if the area was in tension. Compression values of the ultimate strengths were used if the area was in compression.

Table 2.
Values of lamina strengths for E-glass/vinyl ester with v_f=30% (5).

	S_L (MPa)	S_T (MPa)	S_{LT} (MPa)
Tension	584	43	44
Compression	803	187	64

Numerical values of the imposed stresses were extracted from the ABAQUS data output file. Boundary conditions used for this analysis were 1,000 N and a 110-mm horizontal displacement. A displacement of 110 mm was chosen for the analysis because it imposes the highest stress values. This is explained in detail in the literature (4). In all analyzed areas of the composite foot, C_{th} was less than one. The highest C_{th} value was found in the dorsum surface (about 15 mm to the rear of the stiffener) of the composite foot and had a value of 0.036 corresponding to a factor of safety of 27.7. **Figure 9** is a plot of C_{th} *versus* location across the dorsum surface of the foot spanning from medial to lateral. Because the maximum C_{th} value is much less than one, we can conclude that the optimized model will not fail at the specified boundary conditions.

Figure 10 is a plot of C_{th} *versus* load for the area where C_{th} is a maximum. The location of the maximum C_{th} value is at the centerline of the foot section (25 mm), as shown in **Figure 9**. **Figure 10** shows that C_{th} reaches 1 at a load of approximately 5,200 N. Therefore, it can be assumed that the part will fail in the top section of the foot at a load of 5,200 N.

Experimental Failure Test

Figure 11 is a graph of load *versus* displacement as the prosthesis was loaded. A distinct system of cracks was

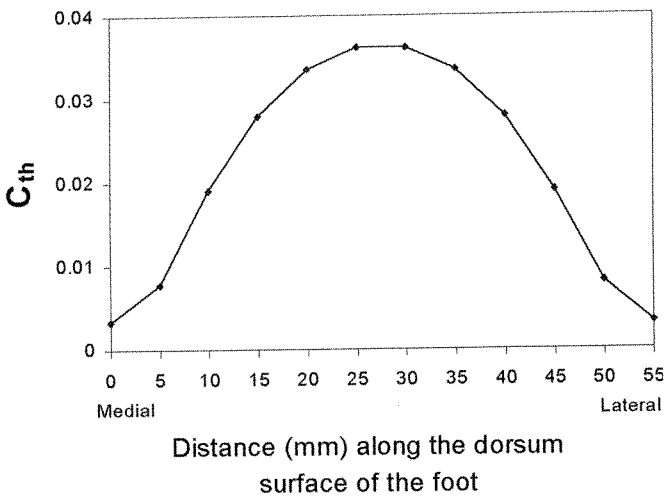

Figure 9.
Tsai-Hill Failure Coefficient *versus* Distance on the dorsum surface of the composite foot spanning from medial to the lateral.

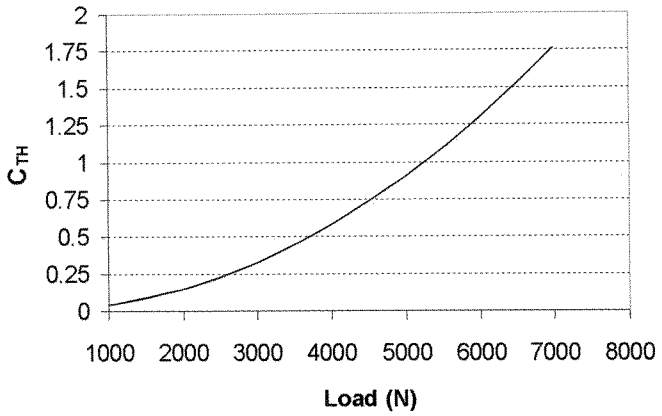

Figure 10.
Tsai-Hill Failure Coefficient *versus* Load on the dorsum surface at the centerline of the composite foot (25 mm).

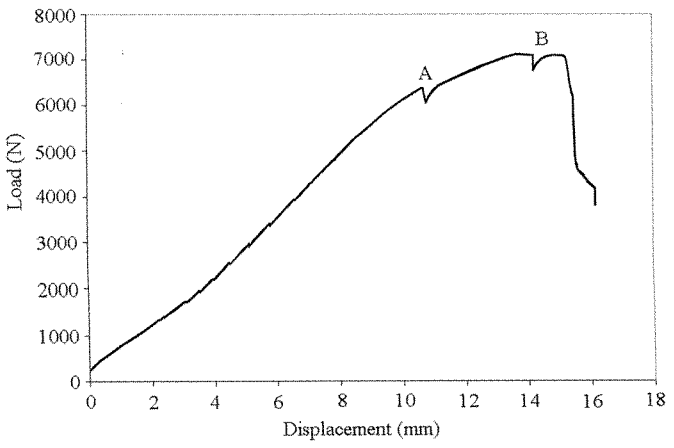

Figure 11.
Load *versus* Displacement as the prosthesis was loaded in compression.

seen in the base of the stiffener section at a load of 6,600 N (point A on **Figure 11**).**Figure 12 (a)** and **(b)** are photographs of the crack, taken during testing at applied loads of (a) 6,600 and (b) 7,000 N. The onset of the crack occurred at the midline of the thickness of the foot (2.5 mm) at the base of the stiffener. It can be assumed that the crack was caused by interlaminar failure at a load of 6,600 N. **Table 3** is a summary of the failure loads for the original prosthesis and the optimized design. If the predicted failure load of 5,200 N is compared with the load at the onset of cracking in the composite prosthesis, good agreement is obtained.

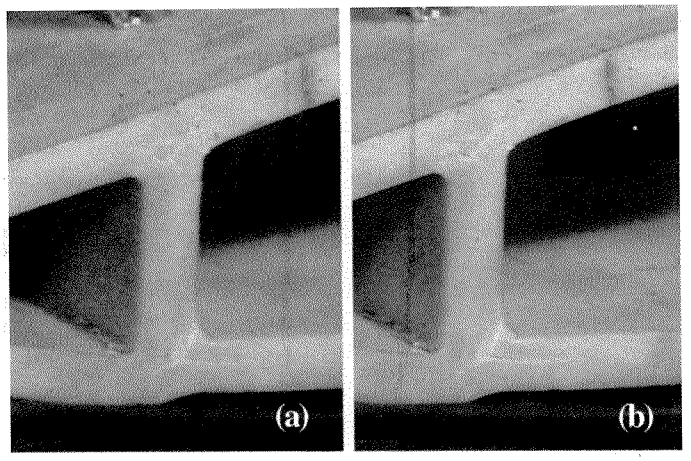

Figure 12.
Photograph of the cracking in the stiffener section of the composite foot at loads of (a) 6600N and (b) 7000N.

Table 3.
Summary of experimental failure loads.

	Optimized Design	Original Design*	ISO Requirement
Failure Load	7,000 N	5,500 N	3,200 N

*=with aluminum stiffeners.

A Comparison of Experimental Data and FE Predictions

To verify the FE model used in the initial analysis of the prosthesis, experimental and numerical values of principle strains were compared. Experimental strains were determined by measuring strain output as load was applied to the prosthesis. Numerical values of principle strains were extracted from the ABAQUS data output file. These values correspond to the element that is at the

exact location of the actual strain gauges. The comparison between the two sets of results assumes boundary conditions of 1,000 N force and horizontal displacement of 10 mm of the superior point of the aluminum leg component.

Figure 13 is a plot of the strain *versus* load for gauge 1. Gauges 2 and 3 have similar plots. Assuming a linear stress-strain relationship, the slope of the line could be used to determine the strain at a load of 1,000 N. Equation 2 was then used to convert the strain measured by the rosettes into strain in the local x and y directions. These values were then used to calculate the principal strains in the location of the gauge using Equation 3.

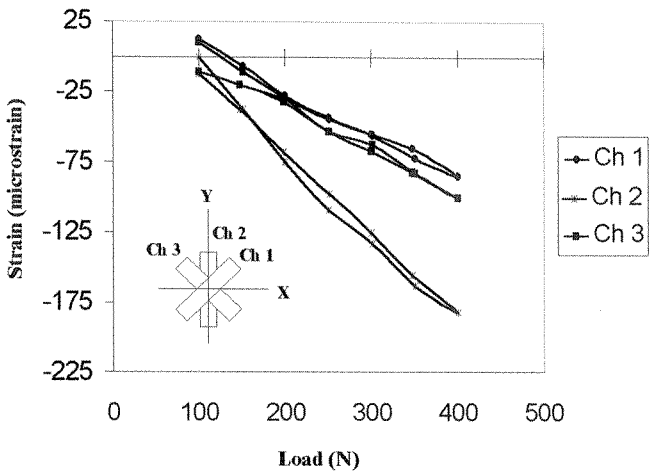

Figure 13.
Strain *versus* Load for Gauge 1.

Comparisons between experimental strain and FE strain results for gauge 1, gauge 2, and gauge 3 are summarized in **Table 4**. The percent error between the two sets of results ranges from a minimum of 3.1 percent to a maximum of 18.6 percent, showing fairly good correlation between the experimental and numerical results. A maximum percent error of 18.6 percent is small, considering the differences between the numerical model and the fabricated prosthesis (summarized below).

Table 4.
Comparison of experimental and modeled principle strains in each gage.

Gage		Experimental	Modeled	Error
1	ε_{p1}	-1,456.6	-1,364.2	6.8
	ε_{p2}	59.6	61.5	3.1
2	ε_{p1}	-560.5	-496.1	13.0
	ε_{p2}	42.1	37.6	11.9
3	ε_{p1}	1,316.6	1,110.3	18.6
	ε_{p2}	82.1	68.2	18.5

Experimental=experimental strain in με; Modeled:moldeled strain in με; Error=percent error.

There are many differences between the FE model of the prosthesis and the fabricated prosthesis. It is very difficult, and often impossible, to exactly simulate the real-life conditions of a composite structure using an FE model. In this study, the differences were subtle but numerous.

First, the FE prosthesis was modeled using a Young's modulus associated with a polyester resin matrix composite system. The actual prosthesis used epoxy as the resin due to the unavailability of polyester resin preprag systems. The elastic moduli of the two differ, but the difference is not considered significant. In reality, the modulus of the system can differ depending on the manufacturing procedure, so it is not possible to choose an accurate modulus for the experimental system without testing the processed material. The composite preprag mats used in the construction of the foot component of the prototype prosthesis were of the standard 2-D-weave type. The Young's modulus of such a composite system depends highly on the amount of resin impregnated in the fiber mat during cure. In the case of mass production by pultrusion, the direction of major fiber loading is along the extrusion direction, normal to the cross-sectional view shown in **Figure 5**. A greater fiber loading gives rise to a stiffer transverse Young's modulus of the mass-produced prosthesis. The effects of fiber loading should be studied quantitatively once an actual pultruded prototype is fabricated.

Secondly, the numerical analysis assumes that the load is applied directly to the top of the leg section. In the actual model, as seen in **Figure 8**, the load is applied offset from the top of the leg section. The load is applied in this manner so that the testing is completed in accordance with the ISO standard for prostheses.

Furthermore, the geometry of the mold used for the fabrication of the prosthesis is not exact due to inconsistencies attributed to the machining process. Thus, the two models (experimental and numerical) are not of identical shape. These inconsistencies are very minor and for the most part can be ignored.

The layup of the fabricated prosthesis was not perfect and voids were present in the final product. The presence of voids most critically effects the mechanical properties of a composite system. Also, there were two areas of fabric buildup on the final prosthesis. This

occurred because the fabric was not wound tightly enough around the mold, a common problem with hand layup of a curved object. The ABAQUS model does not account for these inconsistencies.

Finally, the ABAQUS model requires only one value for the Poisson's ratio, ν_{12}. The estimation of the Poisson's ratio used in the ABAQUS model was not representative of the real composite due to the complexity of contraction effects.

It is important to note that in all three cases the numerical values for strain were lower than that of the actual strain in the area. Although this difference is minimal, it shows that the ABAQUS model does not provide a conservative estimate of the actual strains. This could lead to problems when designing a part based solely on a numerical model. However, the FE analysis did yield results close to the actual values. This shows that ABAQUS is a very valuable design resource, but experimental testing should always follow the numerical analysis.

CONCLUSION

Optimizing the design of the mass-produced transtibial prosthesis will allow for reduced manufacturing cost. Reducing the manufacturing cost will facilitate humanitarian aid programs in providing the prosthesis to people in Third World countries and other areas of need. By replacing the aluminum stiffeners in the original design with a solitary integrated FRP stiffener, the composite foot component can be manufactured in a single step, reducing the cost of the FRP foot component by approximately 35 percent. Thus, it is expected that the total cost of the prosthesis including the FRP foot component, aluminum axial member, aluminum clamps, and heel damper plate will be reduced by 10 percent.

The failure test performed on the fabricated prototype prosthesis shows that it is capable of withstanding a load of 6,600 N before catastrophic failure occurs. This load fully satisfies the static test outlined in the ISO standard 10328 for prostheses and also surpasses the failure load (5,500 N) of the original prosthesis. The optimized design allows for sufficient strength and reduces the cost of manufacturing and thus can be used to replace the original design.

Experimental strain tests were performed on the composite prosthesis and used to verify the numerical results. The maximum percent error, 18 percent, was for gauge 3, which is located on the stiffener section. This amount of error is reasonable due to the differences between the experimental and numerical model. It can be concluded that the results obtained from the ABAQUS model were realistic and that the ABAQUS model is a reliable design tool that can be used if any further design modifications are needed. It is important to note, however, that the strain values obtained from the numerical model were lower than the actual strain in the member.

ACKNOWLEDGMENTS

The authors would like to extend their appreciation to Dr. M. Saito and H. Nakayama for their valuable assistance, the use of their FEM data set, and the use of their experimental jig setup.

REFERENCES

1. Saito M, Sawamura S, Carroll B. Mass-produced prosthesis uses pultruded fiber reinforced plastic. Modern Plastics 1997;74:175–7.
2. Mallick P. Fiber-reinforced composites: materials manufacturing and design. New York: Marcel Dekker Inc.; 1993.
3. ISO Test Standard 10328. International Standards Organization.
4. Hahl J, Taya M, Saito M. Optimization of mass-produced transtibial prosthesis made of pultruded fiber reinforced plastic. Material Science and Engineering-A. [in print]
5. Gibson RF. Principles of composite materials mechanics. New York: McGraw-Hill Inc.; 1994.
6. Dally J, Riley W. Experimental stress analysis. New York: McGraw-Hill Inc.; 1965.
7. Hibbeler R. Mechanics of materials. Engelwood Cliffs, NJ: Prentice-Hall Inc.; 1994.

Submitted for publication December 7, 1999. Accepted February 11, 2000.